INORGANIC CHEMISTRY FRONTIERS

RESEARCH ARTICLE

View Article Online
View Journal | View Issue

Cite this: *Inorg. Chem. Front.*, 2024, **11**, 8331

$(C_3N_6H_7)BF_4{\cdot}H_2O$ and $(C_3N_6H_7)SO_3CH_3{\cdot}H_2O$ with large birefringence induced by coplanar π-conjugated $[C_3N_6H_7]^+$ groups†

Hangwei Jia,[a] Die Xu,[a] Zijian Li,[a,b] Muhammad Arif,[a,b] Yansheng Jiang[a] and Xueling Hou *[a,b]

Received 28th April 2024,
Accepted 20th June 2024

DOI: 10.1039/d4qi01061b

rsc.li/frontiers-inorganic

Birefringent crystals are vital to modern optical devices as they can effectively modulate the polarization of light. Currently, limited by comprehensive properties such as crystal size and birefringence, the design and synthesis of birefringent crystals are challenging, especially in the short-wavelength spectral region. Herein, $(C_3N_6H_7)BF_4{\cdot}H_2O$ and $(C_3N_6H_7)SO_3CH_3{\cdot}H_2O$ were successfully synthesized, and they exhibit large birefringence and short UV cutoff edges (0.37/0.31 at 546 nm and 244/233 nm). Notably, the crystal of $(C_3N_6H_7)BF_4{\cdot}H_2O$ synthesised using a facile solvent growth method is over 20 mm in length. Theoretical analysis suggests that the parallel arrangement of $[C_3N_6H_7]^+$ groups modulated by tetrahedral units induces large optical anisotropy. This work provides promising candidates with exceptional properties for short-wavelength ultraviolet applications.

Introduction

Birefringent crystals are important optoelectronic functional crystals with specific effects and are widely applied in the preparation of optoisolators, polarizers, rotators, delayers and other passive photoelectric devices.[1–3] Commercial crystals in the ultraviolet region primarily include $CaCO_3$,[4] α-BaB_2O_4 (α-BBO)[5] and MgF_2.[6] With the rapid development of modern optics, finding new excellent birefringent crystals has become the focus in order to meet the need of diverse applications.

Generally, the selection of functional building units (FBUs) is very crucial because the chemical composition and spatial arrangement of FBU directly influence the properties of crystals. Owing to the large polarization anisotropy, π-conjugated units, as prime candidates, have been proven to be effective for the large birefringence of the crystal. For instance, $[BO_3]^{3-}$,[7] $[CO_3]^{2-}$,[8] and $[NO_3]^-$,[9] are beneficial for birefringence performance. Besides, some π-conjugated organic groups with planar configuration, such as $[C_2O_4]^{2-}$, $[C_2O_6]^{2-}$, $[C_4O_4]^{2-}$, $[C_6O_6]^{2-}$, $[CO(NH_2)_2]$, $[C(NH_2)_3]^+$, $[C_8H_6BrN_2O]^+$ and $[HN(CH_2COOH)_2]$, show high optical anisotropy, which have greater potential to improve birefringence.[10–15] More recently, inspired by the contribution of B_3O_6 groups toward the large birefringence of the α-BBO crystal, π-conjugated organic units with similar geometric planar configurations to B_3O_6 groups were introduced into the crystal structure to improve birefringence performance. Like $[H_xC_3N_3O_3]^{x-3}$ (x = 0–3), $[C_5H_6ON]^+$, $[C_4H_6N_3]^+$ and $[C_3N_6H_7]^+$ groups[16–21] have been proven to be ideal FBU for constructing large birefringent crystals. Among them, $[C_3N_6H_7]^+$ groups, as excellent birefringent active units, have several advantages. In addition to intrinsic polarization anisotropy, hydrogen bonds formed by the N atoms inside the ring and NH_2 groups outside the ring not only facilitate the coplanar arrangement to improve the birefringent property of the crystal, but are also beneficial to crystal growth to help acquire large-sized crystals. Furthermore, the interatomic distances in the melamine ring are shorter than those in β-BBO, which bring about a greater overlap between the C 2p and N 2p orbitals to generate stronger p_π–p_π interactions and optical anisotropy.[22] Thus far, melamine-based compounds with excellent properties have been synthesized, such as $2(C_3H_7N_6)^+{\cdot}2Cl^-{\cdot}H_2O$,[22] $(H_7C_3N_6)(H_6C_3N_6)ZnCl_3$,[23] $(C_3N_6H_8)PbBr_4$,[20] $(C_3N_6H_8)SnCl_4$,[24] $(C_3N_6H_7)_2SbF_5{\cdot}H_2O$,[25] $(C_3N_6H_7)_2SiF_6{\cdot}H_2O$,[26] and $(C_3N_6H_7)(C_3N_6H_6)HgCl_3$.[27]

[a]*Research Center for Crystal Materials; State Key Laboratory of Functional Materials and Devices for Special Environmental Conditions; Xinjiang Key Laboratory of Functional Crystal Materials; Xinjiang Technical Institute of Physics and Chemistry, Chinese Academy of Sciences, 40-1 South Beijing Road, Urumqi 830011, China. E-mail: xlhou@ms.xjb.ac.cn*

[b]*Center of Materials Science and Optoelectronics Engineering, University of Chinese Academy of Sciences, Beijing 100049, China*

†Electronic supplementary information (ESI) available: The theoretical morphology (Fig. S1), IR spectra (Fig. S2), experiment band structure (Fig. S3), the orientation of $[C3H7N6]^+$ groups in reported compounds (Fig. S4), electronic band structure (Fig. S5), Tables S1–S7: crystallographic data, atomic coordinates, displacement parameters, selected bond lengths and angles, hydrogen bonds. CCDC 2344610 and 2344611. For ESI and crystallographic data in CIF or other electronic format see DOI: https://doi.org/10.1039/d4qi01061b

According to research findings, the arrangement of $[C_3N_6H_7]^+$ groups regulated by different anions can significantly affect crystal properties. It is necessary to introduce suitable anionic units into the crystal configuration to enhance the optical anisotropy of the crystal. However, owing to the narrow band gap between π and π* bonds, it is difficult to balance the birefringence and band gap of the crystal.

To improve this, combining π-conjugated units and non-π-conjugated units should be an effective strategy to design crystals with large optical anisotropy. Generally speaking, π-conjugated units have large hyperpolarizabilities ($|\beta_{max}|$) and polarizability anisotropies (δ) but small HOMO–LUMO gaps. On the contrary, the non-π-conjugated units, such as the tetrahedral $[BO_4]^{5-}$ and $[PO_4]^{3-}$ units,[28,29] have wide HOMO and LUMO band gap, but small $|\beta_{max}|$ and δ.[30] For example, KH_2PO_4 (KDP) has a short UV cutoff edge (174 nm) but shows a small Δn (<0.04 at 1064 nm).[31] Pan's group proposed the non-π-conjugated $BO_{4-x}F_x$ (x = 1–4) groups as the preferred units for deep UV materials, which is conducive to obtaining a large band gap and proper birefringence.[2,32] A series of excellent UV/DUV optical materials, such as $C(NH_2)_3BF_4$,[12] $(C_3N_6H_7)_2(B_3O_3F_4(OH))$,[33] $Li_2B_6O_9F_2$,[32] $LiNaB_6O_9F_2$,[34] $M_2B_{10}O_{14}F_6$ (M = Ca, Sr),[35] $NH_4B_4O_6F$,[36] CsB_4O_6F,[37] $Li_{0.5}Na_{0.5}AlB_2O_4F_2$,[38] and $Ba_2B_9O_{13}F_4{\cdot}BF_4$,[39] has been designed and synthesized. $C_3N_6H_7SO_3NH_2$ was synthesized by Wang's groups, which has a large experimental bandgap of 5.53 eV and a short UV cutoff edge of 206 nm.[40] Similar to the $[SO_3NH_2]^-$ units, the non-π-conjugated $[SO_3CH_3]^-$ units also shows high band gap. For example, $Ba(SO_3CH_3)_2$ has a very short absorption edge of 159 nm and large band gap of 7.8 eV.[41] Therefore, it is necessary to explore the influence of different anions on the $[C_3N_6H_7]^+$ groups arrangement to obtain the large optical anisotropy of the crystal.

Based on the above-mentioned methods, we synthesized two melamine-based compounds, $(C_3N_6H_7)BF_4{\cdot}H_2O$ (**MELBF**) and $(C_3N_6H_7)SO_3CH_3{\cdot}H_2O$ (**MELSC**) using the π-conjugated organic $[C_3N_6H_7]^+$ units and the non-π-conjugated $[BF_4]^-$ and $[SO_3CH_3]^-$ tetrahedral units. Luckily, centimeter-scale crystal (MELBF) was obtained by a facile solvent method. The crystals were characterized with single crystal X-ray diffraction, powder XRD, infrared spectroscopy, UV-visible transmission spectroscopy and thermal analysis. The results show that crystals have excellent optical properties. Furthermore, theoretical calculations uncover the relationship between the structure and properties of the materials.

Experimental

Synthetic procedures

MELBF was prepared using the recrystallization method. A mixture of $C_3N_6H_6$ (40 mmol, 5.04 g) and 40% HBF_4 (8 ml) solution was dissolved in deionized water (100 ml). The solution was kept at 80 °C for 4 h, then cooled to obtain centimeter-sized crystals with 47% yield. The polycrystalline powder was obtained by grinding the crystals. The polycrystalline powder was dissolved in water and recrystallized to obtain the crystals for single crystal structure determination. **MELSC** was prepared using a slow aqueous solution evaporation method. $C_3N_6H_6$ (10 mmol, 1.26 g) and 4 mL 70% methanesulfonic acid solution were dissolved in 80 mL deionized water. The solution was covered with a plastic film with several small holes and evaporated slowly at room temperature. After two weeks, crystallization was observed at the bottom of the solution. Micrometer-sized crystals were selected for single crystal structure determination. The polycrystalline powder was obtained using the aqueous solution method. A mixture of $C_3N_6H_6$ (40 mmol, 5.04 g) and 5 mL of 70% methanesulfonic acid solutions were dissolved in deionized water (100 mL). The solution was kept at 65 °C for 4 h and then cooled to obtain the polycrystalline powder with 40% yield.

Structure determination

The single-crystal diffraction data of the selected single crystals were collected using a Bruker D8 Venture X-ray diffractometer with graphite monochromated Mo Kα radiation. The SAINT and SCALE program was used to integrate the diffraction data and digital absorption correction.[42] SHELXTL program was used to analyze the crystal data.[43] PLATON software was used to verify the crystal symmetry.[44]

Powder XRD

The powder XRD pattern was used to verify the phase purity of the crystals. The diffraction data were collected using a Bruker D2 Phaser XRD diffractometer with Cu Kα radiation (λ = 1.5406 Å). The scan 2θ range was 5 to 70° with a 0.02° step and 1 s scan time.

Thermal analysis

Thermogravimetric analysis (TGA) and differential scanning calorimetry (DSC) were performed on a NETZSCH STA 449F3 Simultaneous Analyzer at a heating rate of 5 °C per minute over a temperature range from 40 to 600 °C.

Infrared (IR) spectrum

The infrared absorption spectra were recorded using a SHIMADZU IRAffinity-1 Fourier transform infrared spectrometer with a resolution of 2 cm^{-1} in the range of 400–4000 cm^{-1}. Crystal samples and KBr were ground and pressed into transparent plates at a mass ratio of 1 : 200.

UV-Vis-NIR diffuse reflectance spectrum

The UV-Vis-NIR diffuse reflectance spectrum and transmittance spectrum of the title compound were recorded at 200–1600 nm using a SolidSpec-3700DUV spectrophotometer.

Birefringence measurements

Birefringence values were measured using a ZEISS Axio Scope polarizing microscope with a Berek compensator. Small crystals were selected for the measurement at 546 nm. The formula was used to calculate the birefringence: $R = |N_e - N_o| = \Delta n \times T$, where R represents the optical path difference, Δn

represents the birefringence, and T represents the thickness of crystal.

Computational description

Theoretical calculations were carried out using the CASTEP software package based on density functional theory (DFT).[45,46] The Perdew–Burke–Ernzerhof (PBE) functional and generalized gradient approximation (GGA) were chosen.[47] H $1s^1$, B $2s^22p^1$, C $2s^22p^2$, N $2s^22p^3$, O $2s^22p^4$, F $2s^22p^5$ and S $3s^23p^4$ electrons were treated as valence electrons. The kinetic energy, Monkhorst–pack mesh, and pseudo-potentials are 900 eV, 4 × 3 × 2, and norm conserving for **MELBF**, and 830 eV, 3 × 2 × 2 and norm conserving for **MELSC**, respectively.

Results and discussion

Crystal growth and chemical phase

By mixing the melamine and tetrafluoroboric acid, colorless block crystals of **MELBF** were easily obtained by the natural cooling crystallization method. The centimeter-scale crystal was grown and is shown in Fig. 1a. The size of the crystal was 24 mm × 4 mm × 0.17 mm. The crystal exhibits a growth habit characterized by two-directional extension, facilitating its facile cultivation in the form of slender stripes. Experimental and calculated XRD patterns were compared to check the purity of the powder (Fig. 1b and c). The experimental XRD patterns of the target compounds are in agreement with the corresponding calculated XRD patterns, indicating the high purity of the target compounds. In accordance with the Bravais–Friedel–Donnay–Harker (BFDH) theory, the theoretical morphology of **MELBF** was calculated with the Mercury program (Fig. S1†).[48]

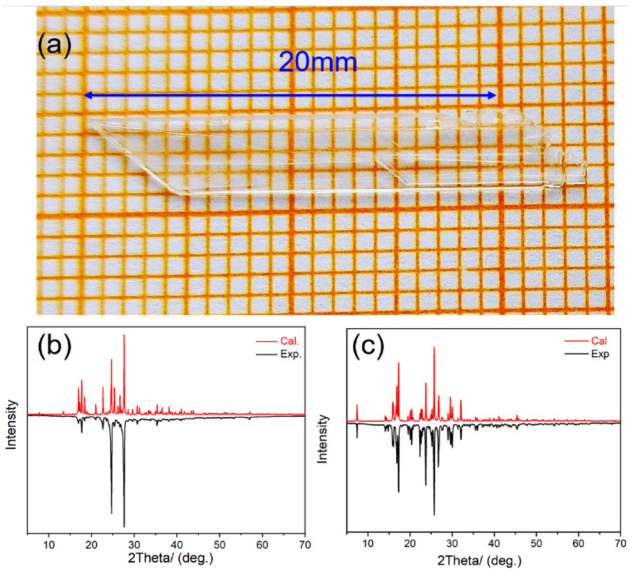

Fig. 1 (a) The as-grown crystals of **MELBF**. Calculated and experimental XRD patterns for **MELBF** (b) and **MELSC** (c).

Crystal structure

Both **MELBF** and **MELSC** crystallize in the centrosymmetric triclinic space groups (no. 2) and have similar structural characteristics. Because the B and F atoms have large thermal vibrations at room temperature, the **MELBF** structure data was collected at 153 K. The data and structural optimization of **MELBF** and **MELSC** are listed in Tables S1–S7.† In the **MELBF** structure, the numbers of independent atoms of C, N, H, B, O and F atoms are 3, 6, 9, 1, 1 and 4, respectively. In the **MELSC** structure, the numbers of independent atoms of C, N, H, S and O atoms are 4, 6, 12, 1 and 4, respectively. As shown in Fig. 2a, the basic structural units of **MELBF** are the planar $[C_3N_6H_7]^+$ group and tetrahedral $[BF_4]^-$ unit. Fig. 2b shows one-dimensional $[C_3N_6H_7]^+$ groups chains formed by hydrogen-bonds. Fig. 2c shows multiple parallel $[C_3N_6H_7]^+$ chains combined by hydrogen bonds from the $[BF_4]^-$ units and $[H_2O]$ units, extending indefinitely within the layer to form two-dimensional planes. The π-conjugated $[C_3N_6H_7]^+$ groups are parallelly arranged so that the π electrons are arranged in order, which enhances the optical anisotropy of the structure. The layers are linked together by hydrogen bonding to form a 3D network structure, as shown in Fig. 2d. Similar to the **MELBF** structure, the basic structural units of **MELSC** consist of planar $[C_3N_6H_7]^+$ groups and tetrahedral $[SO_3CH_3]^-$ units. As shown in Fig. 3b, a one-dimensional chain is formed by the hydrogen-bonded $[C_3N_6H_7]^+$ groups. Multiple parallel $[C_3N_6H_7]^+$ chains extend indefinitely within the layer to form a two-dimensional plane (Fig. 3c). Unlike **MELBF**, the long chains of $[C_3N_6H_7]^+$ are connected with each other by van der Waals force. The layers are connected by hydrogen bonds to form a 3D network structure (Fig. 3d).

Thermal analysis

The TG and DSC tests were performed to investigate the thermal properties of the materials. As shown in Fig. 4a, the DSC curve of **MELBF** shows an endothermic peak at 300 °C. The first weight loss between 210 °C and 309 °C was 36.8%. It is inferred that this may be due to the removal of water molecules and BF_3 gas (cal 37.1%). After that, **MELBF** will experi-

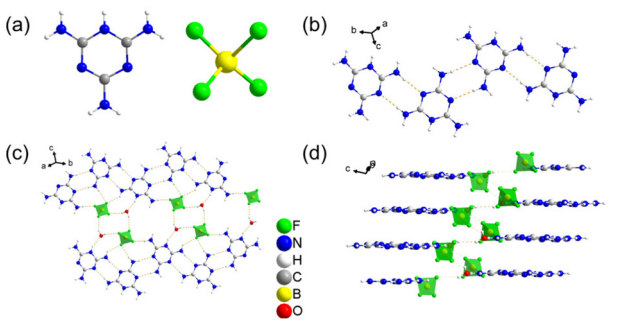

Fig. 2 Crystal structure of **MELBF**. (a) Basic constituent units $[C_3N_6H_7]^+$ and $[BF_4]^-$. (b) The one-dimensional chain formed by $[C_3N_6H_7]^+$ groups. (c) The two-dimensional structure formed by $[C_3N_6H_7]^+$ and $[BF_4]^-$ groups. (d) Three-dimensional structure.

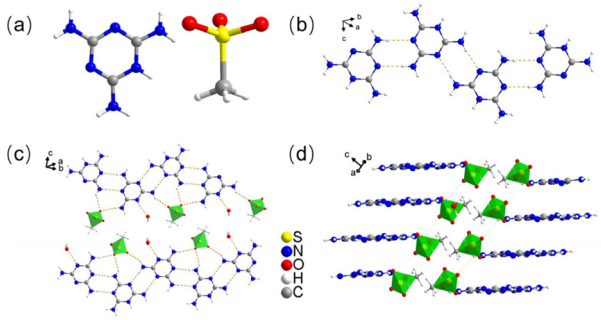

Fig. 3 Crystal structure of **MELSC**. (a) Basic constituent units $[C_3N_6H_7]^+$ and $[SO_3CH_3]^-$. (b) The one-dimensional chain formed by $[C_3N_6H_7]^+$ groups. (c) The two-dimensional structure of $[C_3N_6H_7]^+$ and $[SO_3CH_3]^-$ groups. (d) Three-dimensional structural drawings.

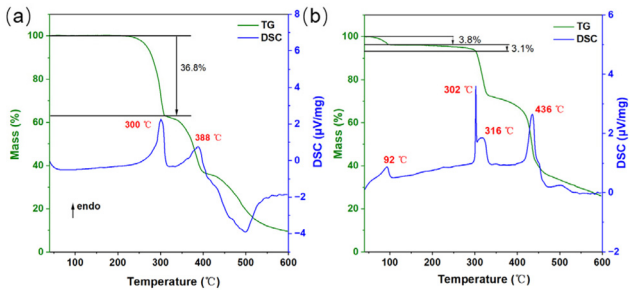

Fig. 4 The TG-DSC curves for (a) **MELBF** and (b) **MELSC**.

ence a continuous loss of weight due to the decomposition of the remaining organic molecules. For the **MELSC**, the weight losses in the first and second segments were 3.8% and 3.1%, respectively, for a total of 6.9%, probably due to the loss of water molecules (cal 7.5%), while the peaks at 316 °C and 436 °C correspond to the decomposition of the residual product (Fig. 4b).

Optical properties

The IR spectra of **MELBF** and **MELSC** were recorded between 4000 and 400 cm^{-1} (Fig. S2†). The peaks located at 3301/3447 cm^{-1} and 1510/1513 cm^{-1} can be specified as the stretching and deformation vibrations of the N–H bond, respectively. The peak at 3189/3165 cm^{-1} is considered to be the hydrogen bond vibration of N–H···X type bonds, where X means N, O or F. The peaks at 1677/1670 cm^{-1} as well as the peaks at approximately 1361/1390, 570/553, 607/618 and 782/779 cm^{-1} demonstrate the NH_2 bending and tensile vibrations in the $[C_3N_6H_7]^+$ groups, respectively.[49]

The UV-vis-NIR transmission and diffuse reflectance spectra indicate that **MELBF** and **MELSC** have wide transparent regions and short ultraviolet cutoff edges (244 and 233 nm, respectively), as shown in Fig. 5 and 6. The experimental band gaps of **MELBF** and **MELSC** are 5.05 and 4.80 eV, respectively (Fig. S3†). The results show that **MELBF** and **MELSC** can be used for UV optical materials.

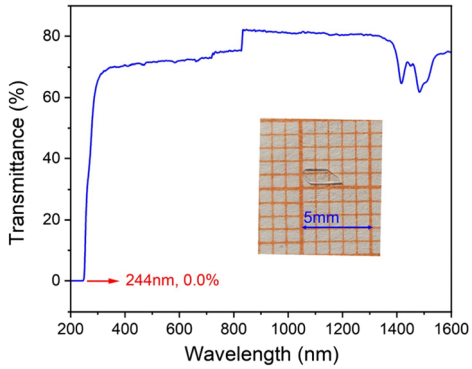

Fig. 5 The UV-vis-NIR transmission spectrum of **MELBF**.

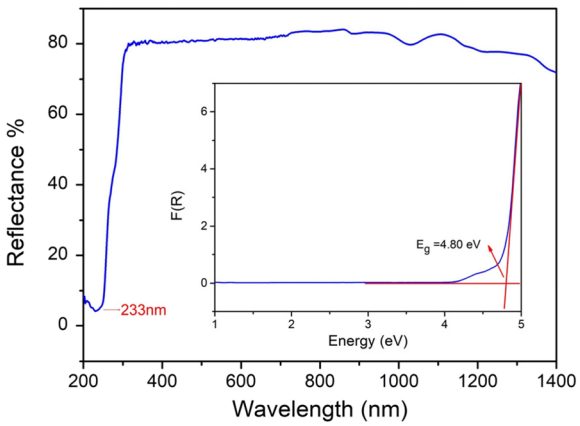

Fig. 6 The UV-vis-NIR diffuse reflectance spectrum of **MELSC**.

Experimental and calculated birefringence

The birefringences of **MELBF** and **MELSC** were calculated, and the birefringence values of **MELBF** and **MELSC** are 0.37 and 0.31 at 546 nm (Fig. 7), respectively. The birefringence of **MELBF** and **MELSC** is larger than that of some birefringent crystals, such as $(C_3N_6H_7)(C_3N_6H_6)HgCl_3$ (0.25@1064 nm),[27] $(C_3N_6H_7)_2SiF_6{\cdot}H_2O$ (0.15@550 nm),[26] and

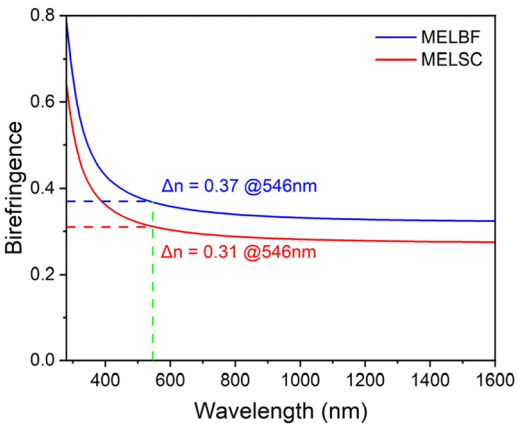

Fig. 7 The calculated birefringence of **MELBF** and **MELSC**.

$(C_3H_7N_6)_6(H_2PO_4)_4(HPO_4)\cdot 4H_2O$ (0.22@1064 nm).[50] The refractive index difference measurement results show that the retardation values for **MELBF** and **MELSC** are approximately equal to 3566 and 2598 nm, respectively. The crystal thicknesses used for the measurements were 11.39 and 12.88 μm, respectively (Fig. 8). The refractive index differences are 0.31 and 0.20 at 546 nm, respectively. The experimental refractive index difference of **MELBF** is close to the calculated value. However, the experimental refractive index difference of **MELSC** is slightly lower than the calculated value. The reason may be that the symmetry of the crystal in the triclinic system is low, and it is difficult to obtain crystal samples with proper optical orientation. Meanwhile, the tested samples do not have the optimal optical orientation; thus, the experimental refractive index difference of **MELSC** crystals is lower than the calculated value.

The relationship between optical property and structure

It is widely known that the birefringence of crystals mainly depends on the density of birefringent active units and arrangement in the structure. For the further explanation of the relationship between $[C_3N_6H_7]^+$ groups and optical properties, $[C_3N_6H_7]^+$ groups' density of compounds was calculated and their orientations were compared. The $[C_3N_6H_7]^+$ densities of **MELBF** and **MELSC** were 3.39×10^{-3} and 3.94×10^{-3} Å^{-3}, respectively, lower than most melamine-based compounds (Table S8†). For example, for $2(C_3H_7N_6)^+\cdot 2Cl^-\cdot H_2O$, $(C_3H_7N_6)_2Cl_2\cdot H_2O$ and $(C_3H_7N_6)F\cdot H_2O$, their $[C_3N_6H_7]^+$ densities were 5.58×10^{-3}, 5.63×10^{-3} and 6.00×10^{-3} Å^{-3}, respectively. Despite the lower density of the $[C_3N_6H_7]^+$ groups in **MELBF** and **MELSC**, they still exhibit high optical anisotropy, which is primarily attributed to the parallel arrangement of $[C_3N_6H_7]^+$ groups in the structure. In order to investigate the influence of the tetrahedral units on the arrangement of the $[C_3N_6H_7]^+$ groups, we compared the arrangement of the $[C_3N_6H_7]^+$ groups in 18 reported melamine-based crystal structures (Fig. S4†). The results show that the $[C_3N_6H_7]^+$ groups are arranged parallel in the crystal structure containing tetrahedral units, such as **MELBF**, **MELSC**, $(C_3H_7N_6)_2SO_4\cdot H_2O$,[50] and $C_3N_6H_7SO_3NH_2$.[40] The band gaps of **MELBF** and **MELSC** are 5.05 and 4.80 eV, respectively, higher than that of 2 $(C_3H_7N_6)^+\cdot 2Cl^-\cdot H_2O$ (4.75 eV), $(C_3H_7N_6)_2Cl_2\cdot H_2O$ (4.70 eV), and $(C_3H_7N_6)F\cdot H_2O$ (4.72 eV) compounds.[22,49] To summarize, it indicates that the introduction of non-π-conjugated tetrahedral units into the crystal structure effectively restricts the density of π-conjugated units, increases the bandgap and regulates the parallel arrangement of $[C_3N_6H_7]^+$ groups. This experimental result is consistent with the principle of π-conjugated confinement proposed by Chen's group.[30]

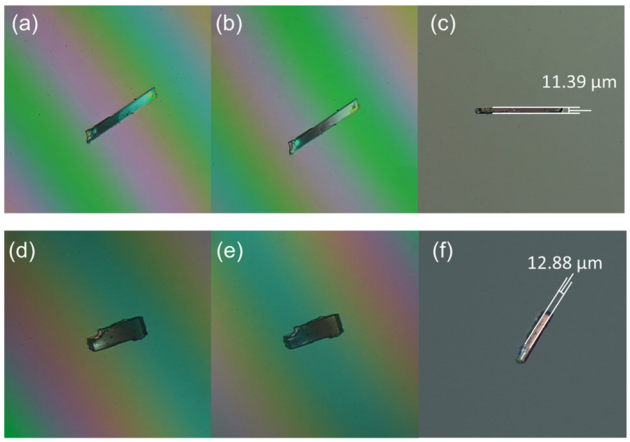

Fig. 8 Refractive index difference measurements for **MELBF** and **MELSC**. **MELBF** single crystal under the (a) positive (up) and (b) negative (down) compensatory rotation; **MELSC** single crystal under the (d) positive (up) and (e) negative (down) compensatory rotation; (c and f) the thickness of **MELBF** and **MELSC**.

Theoretical calculation

In order to provide deep insights into the structure–property relationship, the electronic band structure, density of states (DOS) and electron density difference (EDD) were calculated using the density functional theory in the CASTEP module, based on first principles calculations. The polarizability anisotropy and HOMO–LUMO gap for the $[C_3N_6H_7]^+$, $[BF_4]^-$, and $[SO_3CH_3]^-$ groups were calculated using the DFT method implemented in the Gaussian09 package at the B3LYP/6-31G level.[51,52] The calculated bandgap using the GGA approach are 4.31 eV for **MELBF** and 4.30 eV for **MELSC** (Fig. S5†), lower than the experimental value due to the discontinuity of the exchange correlation energy.[33] The scissor operator with values of 0.74 eV for **MELBF** and 0.50 eV for **MELSC** was used to adjust the conduction bands to their actual level based on the experiment band gap of 5.05 and 4.80 eV, respectively.

The optical properties of the compound are determined by electronic transitions close to the Fermi level. The top region of the valence band is dominated by the C 2p, N 2p, O 2p, F 2p and S 3p orbitals, while the bottom of the conduction band is dominated by the C 2p and N 2p states (Fig. 9). The orbitals of C and N overlap in the conduction and valence bands, suggesting the presence of the strong C–N covalent bond in

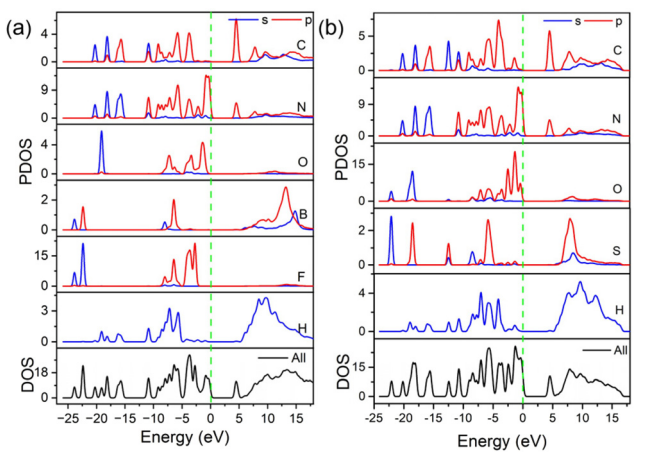

Fig. 9 Total and partial DOS plots for (a) **MELBF** and (b) **MELSC**.

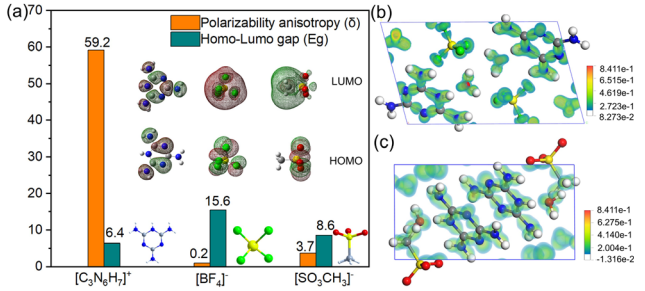

Fig. 10 (a) The polarizability anisotropy and HOMO–LUMO gap for the $[C_3N_6H_7]^+$, $[BF_4]^-$, $[SO_3CH_3]^-$ groups. The EDD of **MELBF** (b) and **MELSC** (c).

the $[C_3N_6H_7]^+$ groups. Moreover, the large overlap between the O 2p, F 2p and N 2p states corresponds to N–H···F and N–H···O hydrogen bonds.

The uniformly distributed π-electron cloud around $[C_3N_6H_7]^+$ groups was observed in Fig. 10b and c, which is favourable for large optical anisotropy. The polarization anisotropy and HOMO–LUMO gap of $[C_3N_6H_7]^+$, $[BF_4]^-$, and $[SO_3CH_3]^-$ groups were calculated (Fig. 10a). The results show that the δ of $[C_3N_6H_7]^+$ groups is 59.2. Considering the planar arrangement of $[C_3N_6H_7]^+$ groups in the crystal structure, it can be inferred that the large birefringence is mainly contributed by the $[C_3N_6H_7]^+$ groups. The HOMO–LUMO gap values of $[BF_4]^-$ and $[SO_3CH_3]^-$ are 15.4 and 8.4, respectively. In addition, the low density of $[C_3N_6H_7]^+$ groups allows the large spacing of the π-conjugated $[C_3N_6H_7]^+$ groups in the structures of **MELBF** and **MELSC**, which is beneficial for increasing the band gap.

Conclusion

Two UV birefringent crystals, $(C_3N_6H_7)BF_4{\cdot}H_2O$ and $(C_3N_6H_7)SO_3CH_3{\cdot}H_2O$, were synthesized by the simple solvent method. The crystal of $(C_3N_6H_7)BF_4{\cdot}H_2O$ is over 20 mm in length. $(C_3N_6H_7)BF_4{\cdot}H_2O$ and $(C_3N_6H_7)SO_3CH_3{\cdot}H_2O$ exhibit short UV cutoff edge (244/230 nm). $(C_3N_6H_7)BF_4{\cdot}H_2O$ exhibits high thermal stability due to strong hydrogen bonding in the crystal structure. The experimental band gaps of $(C_3N_6H_7)BF_4{\cdot}H_2O$ and $(C_3N_6H_7)SO_3CH_3{\cdot}H_2O$ are 5.05 and 4.80 eV, respectively, higher than that of most melamine-based compounds. According to the first-principles calculation, the birefringence of $(C_3N_6H_7)BF_4{\cdot}H_2O$ and $(C_3N_6H_7)SO_3CH_3{\cdot}H_2O$ were calculated to be 0.37 and 0.31@546 nm, respectively. The analyses indicate that the parallel arrangement of planar π-conjugated $[C_3N_6H_7]^+$ groups is mainly responsible for the large optical anisotropy of $(C_3N_6H_7)BF_4{\cdot}H_2O$ and $(C_3N_6H_7)SO_3CH_3{\cdot}H_2O$. The synthesis of UV birefringent crystals using organic π-conjugated planar groups with inorganic non-π-conjugated tetrahedra is a promising direction.

Author contributions

Xueling Hou supervised the research and revision of manuscript. Hangwei Jia designed and performed the experiments, wrote the first draft and revised it. Die Xu did the theoretical calculations. Zijian Li, Muhammad Arif and Yansheng Jiang assisted with the experimental work. All authors participated in the discussion.

Data availability

The authors confirm that the data supporting the findings of this study are available within the article and its ESI.†

Conflicts of interest

The authors declare no conflict of interest.

Acknowledgements

This work was supported by the National Natural Science Foundation of China (22335007, 61835014), the Xinjiang Major Science and Technology Project (2021A01001).

References

1 M. Zhang, D. H. An, C. Hu, X. L. Chen, Z. H. Yang and S. L. Pan, Rational design via synergistic combination leads to an outstanding deep-ultraviolet birefringent $Li_2Na_2B_2O_5$ material with an unvalued B_2O_5 functional gene, *J. Am. Chem. Soc.*, 2019, **141**, 3258.
2 M. Mutailipu, K. R. Poeppelmeier and S. L. Pan, Borates: a rich source for optical materials, *Chem. Rev.*, 2020, **121**, 1130.
3 A. Tudi, S. J. Han, Z. H. Yang and S. L. Pan, Potential optical functional crystals with large birefringence: recent advances and future prospects, *Coord. Chem. Rev.*, 2022, **459**, 214380.
4 G. Ghosh, Dispersion-equation coefficients for the refractive index and birefringence of calcite and quartz crystals, *Opt. Commun.*, 1999, **163**, 95.
5 G. Q. Zhou, J. Xu, X. D. Chen, H. Y. Zhong, S. T. Wang, K. Xu, P. Z. Deng and F. X. Gan, Growth and spectrum of a novel birefringent α-BaB_2O_4 crystal, *J. Cryst. Growth*, 1998, **191**, 517–519.
6 M. J. Bloemer and M. Scalora, Transmissive properties of Ag/MgF_2 photonic band gaps, *Appl. Phys. Lett.*, 1998, **72**, 1676.
7 W. Y. Zhang, Z. Z. Zhang, W. Q. Jin, R. N. Zhang, M. Cheng, Z. H. Yang and S. L. Pan, From borophosphate to fluoroborophosphate: a rational design of fluorine-induced birefringence enhancement, *Sci. China: Chem.*, 2021, **64**, 1498.
8 M. Cheng, W. Q. Jin, Z. H. Yang and S. L. Pan, Large optical anisotropy-oriented construction of a carbonate-nitrate chloride compound as a potential ultraviolet birefringent material, *Chem. Sci.*, 2022, **13**, 13482.

9 Y. X. Song, M. Luo, C. S. Lin and N. Ye, Structural modulation of nitrate group with cations to affect shg responses in $RE(OH)_2NO_3$ (RE = La, Y, and Gd): new polar materials with large NLO effect after adjusting ph values of reaction systems, *Chem. Mater.*, 2017, **29**, 896.

10 T. H. Tong, W. Y. Zhang, Z. H. Yang and S. L. Pan, Series of crystals with giant optical anisotropy: a targeted strategic research, *Angew. Chem., Int. Ed.*, 2021, **60**, 1332.

11 T. T. Huang, Y. Wang, D. Q. Yang and B. B. Zhang, $NACl{\cdot}CH_4N_2O{\cdot}H_2O$: an organic-inorganic hybrid ultraviolet nonlinear optical crystal with optimized comprehensive properties, *Inorg. Chem.*, 2023, **62**, 13626.

12 M. Mutailipu, J. Han, Z. Li, F. M. Li, J. J. Li, F. F. Zhang, X. F. Long, Z. H. Yang and S. L. Pan, Achieving the full-wavelength phase-matching for efficient nonlinear optical frequency conversion in $C(NH_2)_3BF_4$, *Nat. Photonics*, 2023, **17**, 694.

13 Y. R. Shang, H. Y. Sha, Z. J. Wang, R. B. Su, C. He, X. M. Yang and X. F. Long, The birefringence modulation in short–wave ultraviolet sulfates with functional π–conjugated cations and polymerized heteroleptic tetrahedral anions, *Adv. Opt. Mater.*, 2024, 2302844.

14 Y. G. Shen, W. R. Niu, Y. J. Luo, Y. W. Zhou, X. L. Xue and L. Q. Liu, $(C_8H_6BrN_2O)NO_3$: a hybrid nonlinear optical crystal with an appropriate birefringence, *Adv. Opt. Mater.*, 2024, 2400062.

15 Y. H. Zhu, Z. J. Ma, S. C. Li, Z. L. Geng and R. B. Fu, $A_2Pb_3[H_2N(CH_2COO)_2]_3Cl_5$ (A= K, Rb): porous crystals constructed on $[Pb_3Cl_5O_6]$ clusters with comprehensive nonlinear optical performance, *Adv. Opt. Mater.*, 2024, 2400194.

16 D. H. Lin, M. Luo, C. S. Lin, F. Xu and N. Ye, $KLi(HC_3N_3O_3){\cdot}2H_2O$: solvent-drop grinding method toward the hydro-isocyanurate nonlinear optical crystal, *J. Am. Chem. Soc.*, 2019, **141**, 3390.

17 J. Lu, Y. K. Lian, L. Xiong, Q. R. Wu, M. Zhao, K. X. Shi, L. Chen and L. M. Wu, How to maximize birefringence and nonlinearity of π-conjugated cyanurates, *J. Am. Chem. Soc.*, 2019, **141**, 16151.

18 X. H. Meng, X. Y. Zhang, Q. X. Liu, Z. Y. Zhou, X. X. Jiang, Y. G. Wang, Z. S. Lin and M. J. Xia, Perfectly encoding π-conjugated anions in the $RE_5(C_3N_3O_3)(OH)_{12}$ (RE=Y, Yb, Lu) family with strong second harmonic generation response and balanced birefringence, *Angew. Chem.*, 2023, **135**, e202214848.

19 Z. P. Zhang, X. Liu, X. M. Liu, Z. W. Lu, X. Sui, B. Y. Zhen, Z. S. Lin, L. Chen and L. M. Wu, Driving nonlinear optical activity with dipolar 2-aminopyrimidinium cations in $(C_4H_6N_3)^+(H_2PO_3)^-$, *Chem. Mater.*, 2022, **34**, 1976.

20 W. Q. Huang, X. Zhang, Y. Q. Li, Y. Zhou, X. Chen, X. Q. Li, F. F. Wu, M. C. Hong, J. H. Luo and S. G. Zhao, A hybrid halide perovskite birefringent crystal, *Angew. Chem., Int. Ed.*, 2022, **61**, e202202746.

21 J. Lu, X. Liu, M. Zhao, X. B. Deng, K. X. Shi, Q. R. Wu, L. Chen and L. M. Wu, Discovery of nlo semiorganic $(C_5H_6ON)^+(H_2PO_4)^-$: dipole moment modulation and superior synergy in solar-blind uv region, *J. Am. Chem. Soc.*, 2021, **143**, 3647.

22 L. H. Liu, C. L. Hu, Z. Y. Bai, F. F. Yuan, Y. S. Huang, L. Z. Zhang and Z. B. Lin, $2(C_3H_7N_6)^+.2Cl^-.H_2O$: an ultraviolet nonlinear optical crystal with large birefrigence and strong second-harmonic generation, *Chem. Commun.*, 2020, **56**, 14657.

23 L. H. Liu, Z. Y. Bai, L. Hu, D. S. Wei, Z. B. Lin and L. Z. Zhang, A melamine-based organic–inorganic hybrid material revealing excellent optical performance and moderate thermal stability, *J. Mater. Chem. C*, 2021, **9**, 7452.

24 W. Q. Huang, X. L. Wu, B. Ahmed, Y. Q. Li, Y. Zhou, H. Wang, Y. P. Song, X. J. Kuang, J. H. Luo and S. G. Zhao, A hybrid halide lead-free pseudo-perovskite with large birefringence, *Inorg. Chem. Front.*, 2023, **10**, 2039.

25 Y. G. Shen, B. Chen, H. Chen and J. H. Luo, $(C_3N_6H_7)_2SbF_5{\cdot}H_2O$ exhibiting strong optical anisotropy from the optimal arrangement of pi-conjugated $(C_3N_6H_7)^+$ groups, *Inorg. Chem.*, 2022, **61**, 14242.

26 Y. G. Shen, Y. W. Zhou, X. L. Xue, H. L. Yu, S. G. Zhao and J. H. Luo, $(C_3N_6H_7)_2SiF_6{\cdot}H_2O$: an ultraviolet birefringent crystal exceeding the intrinsic energy gap of an organic reagent, *Inorg. Chem. Front.*, 2022, **9**, 5226.

27 Z. Y. Bai, J. Lee, H. Kim, C. L. Hu and K. M. Ok, Unveiling the superior optical properties of novel melamine-based nonlinear optical material with strong second-harmonic generation and giant optical anisotropy, *Small*, 2023, **19**, 2301756.

28 X. M. He, L. Qi, W. Zhang, R. X. Zhang, X. Y. Dong, J. H. Ma, M. Abudoureheman, Q. Jing and Z. H. Chen, Controlling the nonlinear optical behavior and structural transformation with a - site cation in α–$AZnPO_4$ (A= Li, K), *Small*, 2023, **19**, 2206991.

29 L. Wu, R. X. Zhang, Q. Jing, H. Y. Huang, X. M. He, Z. C. Wang and Z. H. Chen, Modulating optical performance by phase transition in a nonlinear optical material β-$Li_2RbBi(PO_4)_2$, *Inorg. Chem. Front.*, 2023, **10**, 4496.

30 L. Xiong, L. M. Wu and L. Chen, A general principle for duv nlo materials: π-conjugated confinement enlarges band gap, *Angew. Chem., Int. Ed.*, 2021, **60**, 25063.

31 V. G. Dmitriev, G. G. Gurzadyan and D. N. Nikogosyan, *Handbook of nonlinear optical crystals*, Springer, 2013.

32 B. B. Zhang, G. Q. Shi, Z. H. Yang, F. F. Zhang and S. L. Pan, Fluorooxoborates: beryllium free deep ultraviolet nonlinear optical materials without layered growth, *Angew. Chem., Int. Ed.*, 2017, **56**, 3916.

33 C. C. Jin, F. M. Li, Z. H. Yang, S. L. Pan and M. Mutailipu, $[C_3N_6H_7]_2[B_3O_3F_4(OH)]$: a new hybrid birefringent crystal with strong optical anisotropy induced by mixed functional units, *J. Mater. Chem. C*, 2022, **10**, 6590.

34 X. J. Li, Z. L. Chen, F. M. Li, F. F. Zhang, Z. H. Yang and S. L. Pan, $LiNaB_6O_9F_2$: a promising UV NLO crystal having fluorine directed optimal performances and double interpenetrating $^3[B_6O_9F_2]_\infty$ networks, *Adv. Opt. Mater.*, 2023, **11**, 2202195.

35 M. Luo, F. Liang, Y. X. Song, D. Zhao, F. Xu, N. Ye and Z. S. Lin, $M_2B_{10}O_{14}F_6$ (M= Ca, Sr): two noncentrosymmetric alkaline earth fluorooxoborates as promising next-generation deep-ultraviolet nonlinear optical materials, *J. Am. Chem. Soc.*, 2018, **140**, 3884.

36 G. Q. Shi, Y. Wang, F. F. Zhang, B. B. Zhang, Z. H. Yang, X. L. Hou, S. L. Pan and K. R. Poeppelmeier, Finding the next deep-ultraviolet nonlinear optical material: $NH_4B_4O_6F$, *J. Am. Chem. Soc.*, 2017, **139**, 10645.

37 X. F. Wang, Y. Wang, B. B. Zhang, F. F. Zhang, Z. H. Yang and S. L. Pan, CsB_4O_6F: a congruent melting deep ultraviolet nonlinear optical material by combining superior functional units, *Angew. Chem., Int. Ed.*, 2017, **56**, 14119.

38 Z. T. Yan, D. D. Chu, M. Zhang, Z. H. Yang and S. L. Pan, $Li_{0.5}Na_{0.5}AlB_2O_4F_2$: fluoroaluminoborate with aligned $^1{}_\infty[BO_2]$ chain induced by unprecedented $[AlO_3F_3]^{6-}$ species features enhanced birefringence, *Adv. Opt. Mater.*, 2023, **11**, 2202353.

39 H. Pei, X. F. Wang, J. Zhang, F. F. Zhang, Z. H. Yang and S. L. Pan, $Ba_2B_9O_{13}F_4{\cdot}BF_4$: first fluorooxoborate with unprecedented infinite $[B_{18}O_{26}F_8]$ tubes and deep-ultraviolet cutoff edge, *Sci. China: Chem.*, 2023, **66**, 1073.

40 D. Y. Dou, Q. Shi, Y. J. Bai, C. Chen, B. B. Zhang and Y. Wang, $C_3N_6H_7SO_3NH_2$: non-π-conjugated tetrahedra decoupling π-conjugated groups achieving large optical anisotropy and wide band gap, *Mater. Chem. Front.*, 2023, **7**, 5924.

41 H. T. Tian, C. S. Lin, X. Zhao, F. Xu, C. Wang, N. Ye and M. Luo, $Ba(SO_3CH_3)_2$: a deep-ultraviolet transparent crystal with excellent optical nonlinearity based on a new polar non-π-conjugated nlo building unit $SO_3CH_3^-$, *CCS Chem.*, 2023, **5**, 2497.

42 *Version 7.60 A*, Bruker Analytical X-ray Instruments, 2000.

43 G. M. Sheldrick, A short history of shelx, *Acta Crystallogr., Sect. A. Found. Crystallogr.*, 2008, **64**, 112.

44 A. Spek, Single-crystal structure validation with the program platon, *J. Appl. Crystallogr.*, 2003, **36**, 7.

45 J. Heyd and G. E. Scuseria, Efficient hybrid density functional calculations in solids: assessment of the heyd–scuseria–ernzerhof screened coulomb hybrid functional, *J. Chem. Phys.*, 2004, **121**, 1187.

46 V. Milman, K. Refson, S. J. Clark, C. J. Pickard, J. R. Yates, S. P. Gao, P. J. Hasnip, M. I. J. Probert, A. Perlov and M. D. Segall, Electron and vibrational spectroscopies using DFT, plane waves and pseudopotentials: Castep implementation, *J. Mol. Struct.*, 2010, **954**, 22.

47 J. P. Perdew, K. Burke and M. Ernzerhof, Generalized gradient approximation made simple, *Phys. Rev. Lett.*, 1996, **77**, 3865.

48 J. D. H. Donnay and D. Harker, A new law of crystal morphology extending the law of bravais, *Am. Mineral.*, 1937, **22**, 446.

49 Y. G. Shen, L. Ma, G. F. Dong, H. L. Yu and J. H. Luo, B-$(C_3H_7N_6)_2Cl_2{\cdot}H_2O$ and $(C_3H_7N_6)F{\cdot}H_2O$: two uv birefringent crystals induced by uniformly aligned structural groups, *Inorg. Chem. Front.*, 2023, **10**, 2022.

50 S. F. Li, L. Hu, Y. Ma, F. F. Mao, J. Zheng, X. D. Zhang and D. Yan, Noncentrosymmetric $(C_3H_7N_6)_6(H_2PO_4)_4(HPO_4){\cdot}4H_2O$ and centrosymmetric $(C_3H_7N_6)_2SO_4{\cdot}2H_2O$: exploration of acentric structure by combining planar and tetrahedral motifs via hydrogen bonds, *Inorg. Chem.*, 2022, **61**, 10182.

51 S. J. Clark, M. D. Segall, C. J. Pickard, P. J. Hasnip, M. I. J. Probert, K. Refson and M. C. Payne, First principles methods using CASTEP, *Z. Kristallogr. – Cryst. Mater.*, 2005, **220**, 567.

52 M. C. Payne, M. P. Teter, D. C. Allan, T. A. Arias and J. D. Joannopoulos, Iterative minimization techniques for ab initio total-energy calculations: molecular dynamics and conjugate gradients, *Rev. Mod. Phys.*, 1992, **64**, 1045.

